THE ASTROPHYSICAL JOURNAL, 436:183–193, 1994 November 20

NGC 3603 AND ITS WOLF-RAYET STARS: GALACTIC CLONE OF R136 AT THE CORE OF 30 DORADUS, BUT WITHOUT THE MASSIVE SURROUNDING CLUSTER HALO[1]

ANTHONY F. J. MOFFAT
Département de Physique, Université de Montréal, C.P. 6128, Succ. Centre-ville, Montréal, Qc, Canada H3C 3J7, and Observatoire du Mont Mègantic;
e-mail: moffat@astro.umontreal.ca

AND

LAURENT DRISSEN AND MICHAEL M. SHARA
Space Telescope Science Institute, 3700 San Martin Drive, Baltimore, MD, 21218; e-mail: drissen@stsci.edu, shara@stsci.edu
Received 1994 February 4; accepted 1994 May 24

ABSTRACT

HST/PC images of the dense stellar cluster at the center of the Galaxy's most massive visible H II region, NGC 3603, reveal remarkable similarity to the dense core R136 in the Local Group's most massive Giant H II region, 30 Dor. The projected star density for stars brighter than $M_V = -5.0$ in both objects increases inwards to the last data bin in both objects at $r = 0.033$ pc with a power-law of slope close to -1.8. Even the central star density in NGC 3603 is similar to that found in R136. Outside $r \approx 1$ pc, NGC 3603 plummets to zero density, at least for its massive stars, while 30 Dor continues to decrease with similar power-law slope out to $r \approx 130$ pc. Narrowband He II 4686 Å images reveal that NGC 3603 contains three WR stars; they stand out as the brightest members of NGC 3603, all located within the central 0.1 pc. However, while R136 also contains three bright WR stars within 0.1 pc of its center, they are almost a magnitude fainter than NGC 3603's WR stars. Reasons for these differences are probably related to the different environments and ages of the two objects.

Subject headings: H II regions — ISM: individual (NGC 3603) — open clusters and associations: individual (NGC 3603) — stars: Wolf-Rayet

1. INTRODUCTION

NGC 3603 appears to be the densest concentration of early-type, massive stars known in the Galaxy, with the possible exception of the Galactic center cluster (GCC), although the latter seems to consist of a mixture of stars of different ages (Rieke & Rieke 1988; Krabbe et al. 1991). NGC 3603 also enjoys the distinction of being the most massive *visible* giant H II region (GHR) in the Galaxy. The radio GHR W49A is more massive but is not seen in the visible: Welch et al. 1987.) NGC 3603 has often been compared in outward appearance with 30 Doradus, the most massive GHR in the Local Group system of galaxies, starting with the work of Walborn (1973). This is remarkable, because both objects are at quite different distances (~7 kpc for NGC 3603, ~50 kpc for 30 Dor in the LMC). Taken at face value, it would thus appear that NGC 3603, and especially its core, HD 97950, must be considerably more compact than even 30 Dor's core, R136. Indeed, a ground-based upper limit to NGC 3603's core radius $r_c < 0''.7$ (0.02 pc) (Moffat, Seggewiss, & Shara 1985, hereafter MSS) makes it possibly even more extreme than R136, with $r_c < 0''.25$ (0.06 pc), based on recent *HST*/PC data (Campbell et al. 1992). By comparison, the GCC has $r_c = 0.15 \pm 0.05$ pc (Eckart et al. 1993). Based on the light distribution, MSS concluded that the core of NGC 3603 must be $\approx 300\times$ denser than R136's core. This yields a shorter relaxation time for NGC 3603, and hence might explain why objects like NGC 3603 are so rare in the Galaxy. Note that the *total* mass of 30 Dor exceeds that of NGC 3603 by a factor ~3 in stars and ~50 in H II gas (MSS).

Although MSS could barely resolve the central visual components A, B, C in NGC 3603 (van den Bos 1928; component A has subsequently been broken up into unresolved components A1, A2, A3 at 0''.09 resolution by Hofmann & Weigelt's 1986 speckle data), their on- versus off-line He II 4686 Å data yielded 2–3 (most likely 3) Wolf-Rayet (WR) stars. In fact, they claimed that there was most likely one WR star of type WNL in each of A, B, and C, one (or even two) of which are spectroscopic binaries (Moffat & Niemela 1984), as in R136 (MSS). Note that WR stars are easily detected, discrete probes of the initially most massive stars, especially in crowded regions of recent star formation (ages 3–6 million years).

From previous work, several questions still remain unanswered:

1. Why is the core of NGC 3603 so dense, or in fact is it really so dense? (Note that its structure was studied by MSS, based on light distribution as opposed to star counts; both need not lead to the same conclusion: cf. the GCC, Eckart et al. 1993.)

2. Why are all of NGC 3603's WR stars located close to its center, while R136 contains only ~20% of 30 Dor's WR stars (MSS)? Is this due to small number statistics? Is NGC 3603 more relaxed than 30 Dor?

3. Are the speckle components A1, A2, A3, B further resolvable into still fainter stars?

Clearly, there is a need for higher resolution imagery of NGC 3603, reaching fainter than just the four main speckle components (two more added later by Baier et al. 1988). Understanding close GHRs with high stellar density, like NGC 3603, may provide important clues for distant, unresolvable extragalactic GHRs, including some active galactic nuclei and our own Galactic center. We report here on the results of *Hubble Space Telescope* Planetary Camera imagery of NGC

[1] Based on observations with the NASA/ESA Hubble Space Telescope, obtained at the Space Telescope Science Institute, which is operated by AURA, Inc., under NASA contract NAS 5-26555.

3603, using two filters, one close to broadband B, the other narrowband, centered on He II 4686, to locate and count the WR stars.

2. OBSERVATIONS AND REDUCTION

We have obtained images of NGC 3603 in 1991 August in both broadband F439W (close to broadband B; exposures of 1 and 5 s) and narrowband F469N (FWHM = 20° Å, centered on He II 4686 Å, to isolate WR stars; exposures of 14 and 100 s, giving comparable total counts as in the F439W images). Bias subtraction and flatfield corrections were applied according to the standard STScI pipeline. Unfortunately, part of NGC 3603 was located at the interface between the CCD chips, where the PSF variations cannot be modeled with any precision. Thus, the worst parts of the F439W and F469N images in the interchip region were replaced by unaffected small strips of archived images in *V* (F555W) and F469N, scaled in magnitude to match the former image pair.

We show in Figure 1 an overview of the complete PC field right to the edge of all four chips (after proper alignment), in the F439W filter. Stars outside the central crowded region are identified. A 10″ × 10″ blow-up of this is compared to a ground-based CCD image at the same scale and orientation in Figure 2. Figure 3*a* shows a zoom of the central 13″ × 13″ subfield in Figure 1, with a separate identification chart (Fig. 3*b*) to avoid confusion.

Using DAOPHOT, magnitudes were obtained with aperture photometry (cf. Table 1). In the case of the F439W filter, the magnitudes were converted by zero-point shift to standard *B*-values calibrated by stars in common with the ground-based work of Melnick, Tapia, & Terlevich (1989; hereafter MTT). Figure 4*a* shows the comparison between our *B*-values and those of MTT in the form of a color equation (data in Table 2). This plot reveals that there is no significant color term (as expected: see Harris et al. 1991), and the scatter is 0.16 mag for an average magnitude difference. Assuming the ground-based data to be more precise, this probably well represents the typical scatter of the *HST* photometry. Magnitude difference versus magnitude is shown in Figure 4*b*, where no correlation is apparent.

Table 1 gives a list of the magnitudes and *HST* pixel coordinates of detected stars down to the 3 σ level above the background. The F469N magnitudes were obtained by forcing a mean difference of zero with the calibrated *B*-magnitudes,

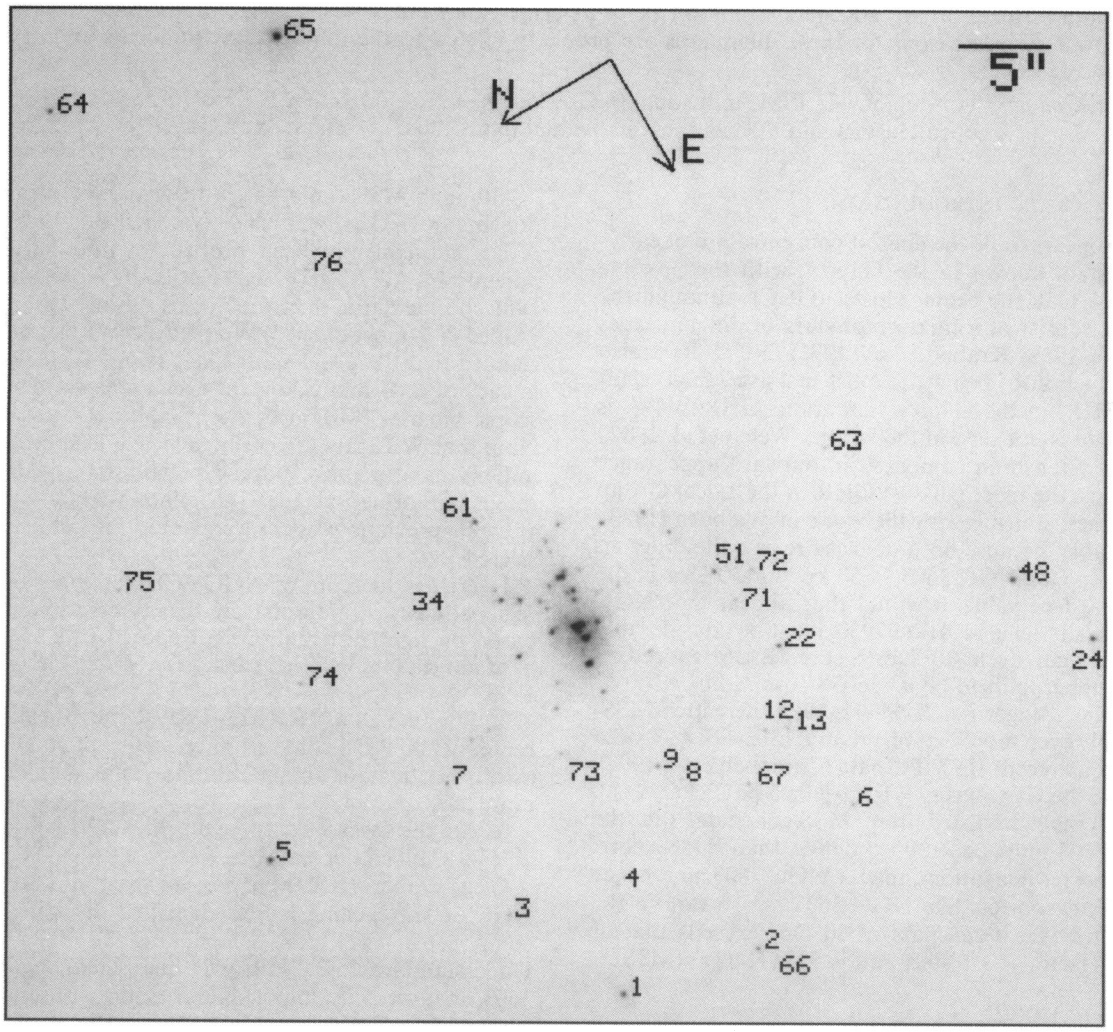

FIG. 1.—Full *HST*/PC field in F439W (~*B*) filter of NGC 3603. Stars outside the central crowded region are identified by HST numbers in Table 1. No deconvolution has been carried out here. One pixel corresponds to 0.″0439.

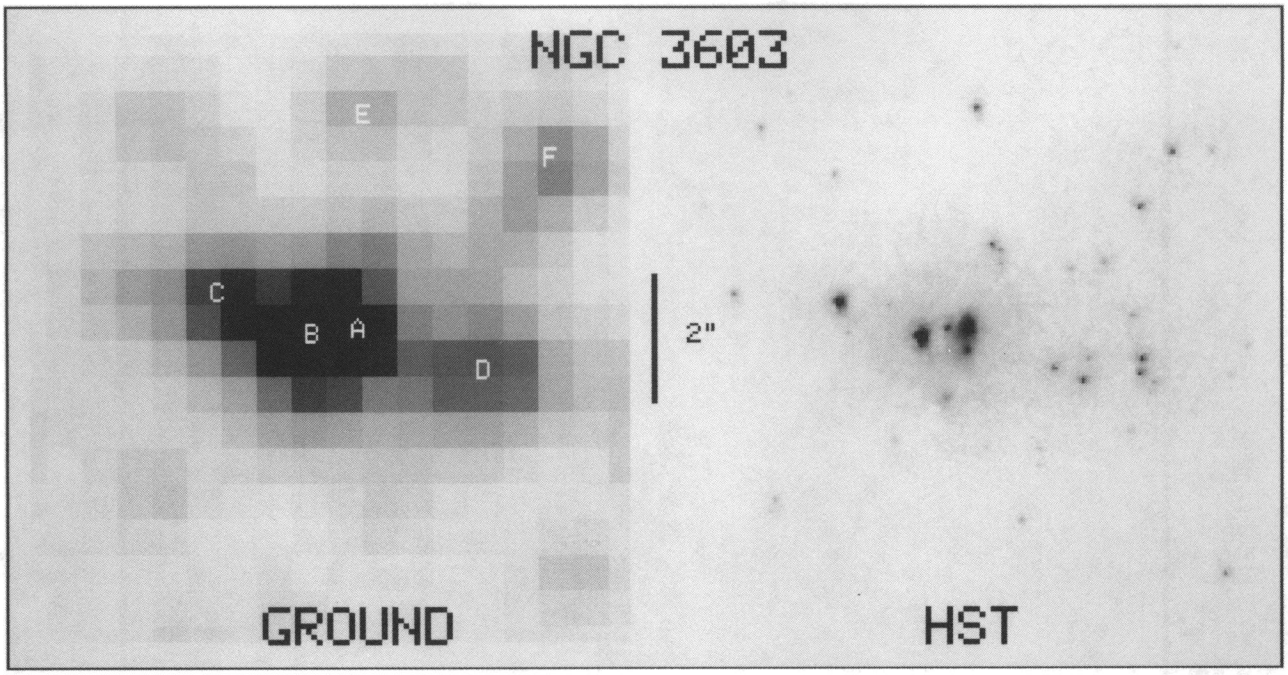

FIG. 2.—Central 10″ × 10″ of a *B*-band ground-based CCD image of NGC 3603 (same source as Moffat et al. 1985), compared at the same scale and orientation to the central *HST*/PC image in Fig. 1. North is up, East to the left. Van den Bos components A-F are indicated.

except for He II 4686 Å emission-line stars (see below). Note that speckle magnitudes of components A1, A2, A3, B are similar to those presented in Table 1, except that they are less precise. (There are also some large differences in magnitude between the two speckle papers by Baier, Ladebeck, & Weigelt 1985 and Hofmann & Weigelt 1986). Stars A1, A2, A3, B, C are very bright compared to all other stars in the field, yet they show no direct evidence for multiplicity at the 0.″1 level; we will assume they are single in the following discussion, although this point needs to be pursued at a future date with even better spatial resolution.

3. RESULTS AND DISCUSSION

3.1. *WR and Of Star Content*

From the scaled difference image (F469N − F439W) in Figure 5 and the plot of magnitude differences in Figure 6, we see a very significant He II 4686 Å emission excess in stars A1, B, and C. We now calculate the net 4686 Å emission in absolute units for these three stars, based on the above magnitudes and assuming a distance of 7 kpc, reddening $A_{4686\,\text{Å}} = 3.83E_{B-V}$, with $E_{B-V} = 1.44$ typical for stars in the central region of NGC 3603 (MTT). We find net He II 4686 Å fluxes of (5, 8, 2) × 10^{36} ergs s^{-1} for stars A1, B, C, respectively. These compare with a mean of 1.7 × 10^{36} ergs s^{-1} and a maximum (R144 in 30 Dor) of 7 × 10^{36} ergs s^{-1} for WNL stars (Vacca 1990). Thus, taken as a single WR stars, A1, B, and C in NGC 3603 correspond to some of the more extreme WNL stars, as found in 30 Dor, but outside R136 (Campbell et al. 1992). These results confirm and refine those found previously from ground-based observations of NGC 3603 by MSS. Note also, that the core of NGC 3603 contains one short-period WNL binary and a possible long period one (Moffat & Niemela 1984). However, this alone does not necessarily explain the high brightness of A1 and B in NGC 3603, since most WNL binaries are SB1 systems in which the companion is unseen in the combined spectrum, and hence contributes little to the total light. Although our *completeness* detection limit is $M_V \approx -5$ (see below), we would have *detected* fainter WR stars (e.g., down to $M_V \approx -3$) easily, because of their high emission-line fluxes. We conclude that, among WR stars, NGC 3603 contains only intrinsically bright WNL stars.

Weaker net 4686 Å emission is found (cf. Fig. 6) for stars HST 2 [O5 V(f)], 39 [O5.5 III(f); note that the ground-based spectrum is a composite of stars HST 38, 39, and 43], and 48 [O6 If]. Note that stars HST 22 [O5 III(f)] and 51 [(O4 V(f)] apparently do not have as much He II 4686 Å emission as the above 3 O(f), Of stars.

3.2. *Spatial Density Profile*

Figure 7 shows a plot of star number versus *B*-magnitude for all stars detected on the F439W image (Table 1). A turnover occurs at $B \approx 15.0$, implying that this is the limit of completeness. The mean apparent modulus $V - M_V = 18.86$, mean reddening $E_{B-V} = 1.44$, and mean color for the bright blue members $M_B - M_V = -0.3$ (Moffat 1983), leads to an intrinsic completeness limit of $M_V = B - (V - M_V) - E_{B-V} - (M_B - M_V) = B - 20.0 = -5.0$. For the remaining statistical study, we limit the discussion to stars with $B \leq 15.0$.

In order to locate the cluster center, we carry out strip counts (on all stars to $B = 15.0$) independently in both directions (cf. Fig. 8). The center of symmetry is found to lie at x_c, $y_c = 695$, 495 pixels, close to A1—the brightest star in the cluster. With these coordinates, we investigate how stars of different absolute magnitude are distributed radially from the cluster center in Figure 9 (cf. also Table 3), along with a similar plot for R136, based on the *HST* results of Campbell et al. (1992). Here, we see that, out to $r \sim 1$ pc, NGC 3603 behaves like R136, except that NGC 3603's three central WR stars are ~1 mag brighter than R136's three central WR stars. Outside $r \sim 1$ pc, the 30 Dor field exhibits an extended halo dominated

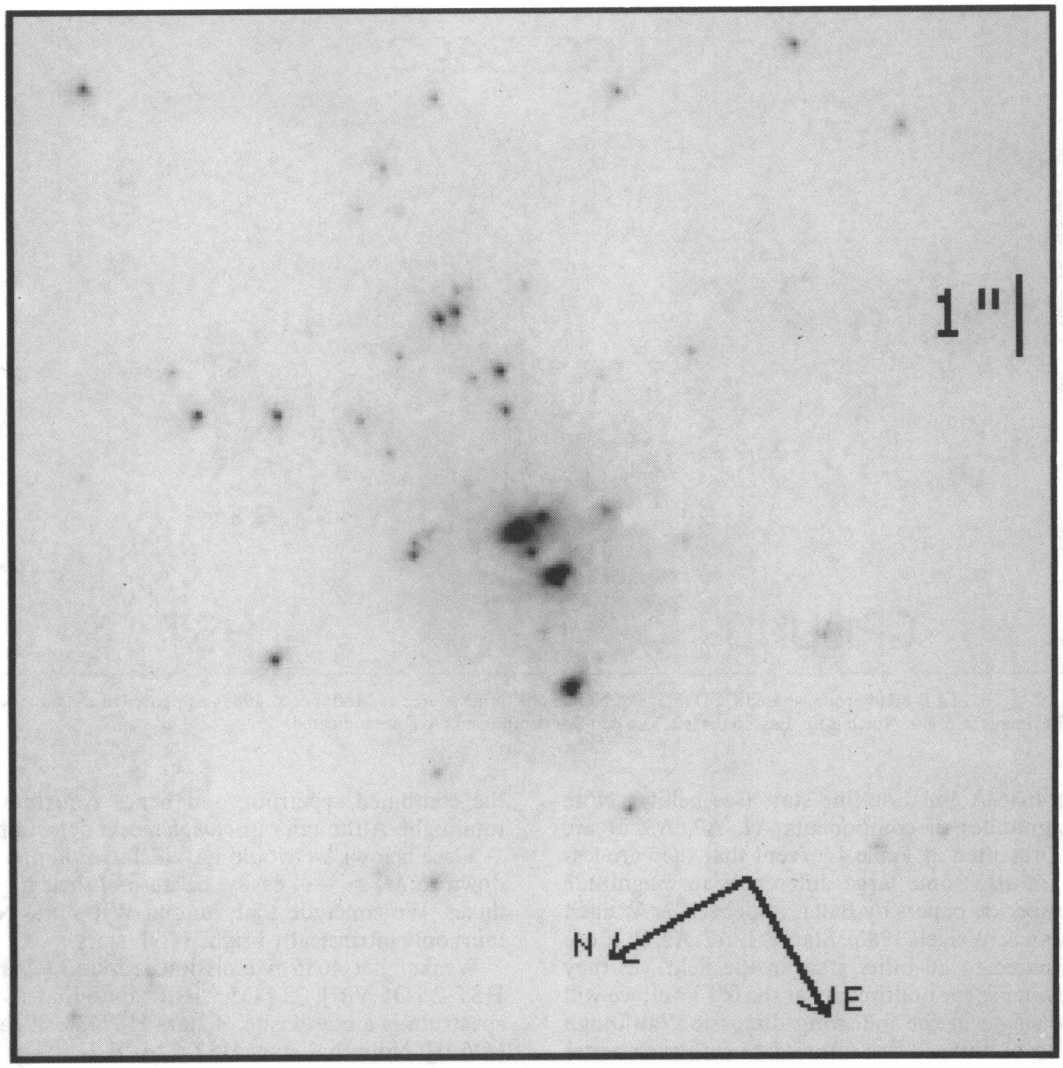

FIG. 3a

FIG. 3.—(*a*) Central zoom of Fig. 1. (*b*) As in (*a*), showing identifications. A narrow rectangular strip of this image has been replaced by an intensity-scaled strip from the archive F555W image for the stars A1, A2 (= *HST* 30, 31), which fell close to the inter-chip region of the Planetary Camera on the F439W image.

by member stars brighter than in R136. Such a halo is completely missing in NGC 3603.

Using the same data as in Figure 9, we show in Figure 10 a radial plot of star number density for NGC 3603 and R136 and their surroundings out to $r \sim 4$ pc (cf. Table 4). Both clusters are limited to stars brighter than the same limit, $M_V = -5.0$. This limit is close to the main-sequence turn-off in both cases (O4 in NGC 3603, O3 in 30 Dor/R136), so that detailed differences in star counts, due to post–main-sequence evolution between the two clusters are expected to be minimized. Figure 10 shows no significant evidence for a central flattening (core) in either case, as expected for the youngest clusters (cf. Elson, Freeman, & Lauer 1990). A power-law (linear in log-log), weighted fit, of the form $\log \sigma = c_1 + c_2 \log r$, between projected star density and projected radius from the cluster center in Figure 10, yields, c_1, $c_2 = 0.10 \pm 0.12$, -2.08 ± 0.12 for NGC 3603 (out to $r = 1$ pc) and 0.33 ± 0.05, -1.65 ± 0.08 for R136/30 Dor (out to $r = 4$ pc). The slope found here (c_2) based on star *counts* for R136/30 Dor is similar to that found by Campbell et al. (1992) based on total *light* distribution (-1.72 ± 0.06). Based on the WR star population alone in 30 Dor, Moffat et al. (1987) found $c_2 \approx -2$ extending from R136 out to $r \sim 130$ pc. Note the remarkable similarity in the spatial distribution of the WR stars in each of NGC 3603 and R136. Small numbers prevent us from judging whether relaxation effects have made the more massive (progenitors of the) WR stars sink more to the center than other stars; nevertheless, their strong central concentration is remarkable.

Not only do NGC 3603 and R136 show remarkable similarity in their projected radial star density profiles for their massive stars. Both objects show similar projected central density as well, within the errors. If anything, however, NGC 3603 has a central density that is at least as great as in R136, contrary to the claim of Campbell et al. (1992).

Formal conversion of spatial density $\rho(r)$ into projected surface density $\sigma(r)$, or vice versa, can be made by integrating ρ along the line of sight z:

$$\sigma(r) = \int_{-\infty}^{\infty} \rho(R) dz \ ,$$

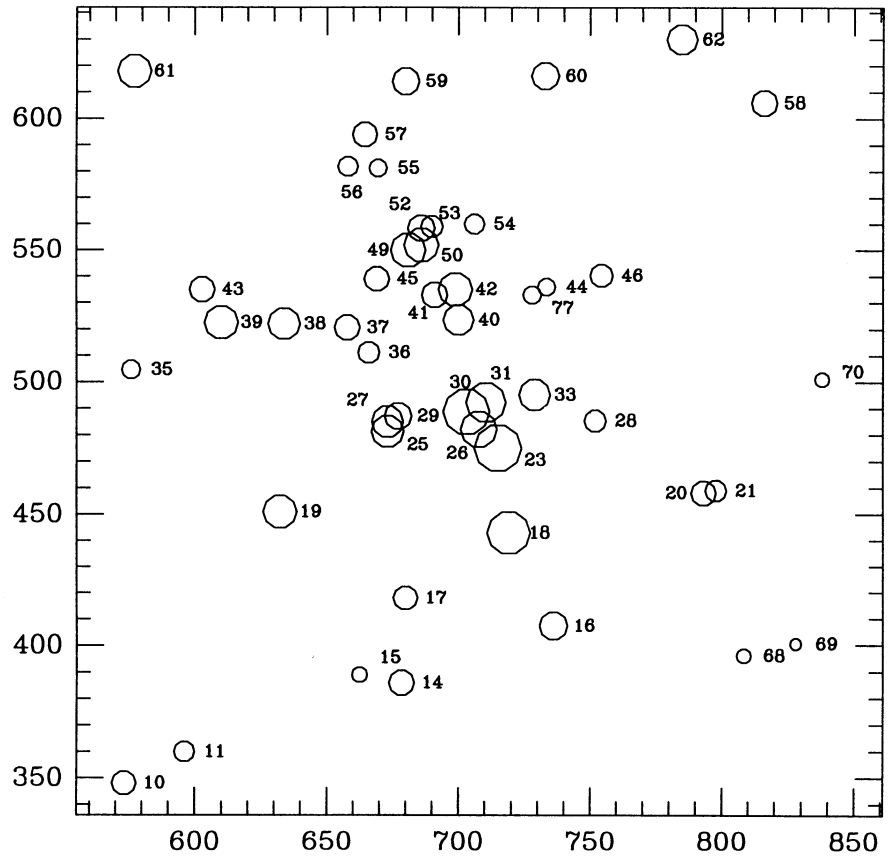

FIG. 3*b*

where $z^2 = R^2 - r^2$, r = constant. If we adopt a spatial power law of the form

$$\rho(R) = kR^{\alpha} ,$$

with k, α = constants, integration of the above equation yields

$$\sigma(r) = \pi k f(\alpha) r^{\alpha+1} ,$$

i.e., also a power law, as observed, where

$$f(\alpha) = \pi^{-1} \int_{-\pi/2}^{\pi/2} d\theta / \cos^{\alpha+2} \theta ,$$

in which, e.g., $f(-2) = 1$. In the above notation $c_1 = \log [\pi k f(\alpha)]$ and $c_2 = \alpha + 1$. Using subscript a for NGC 3603 and

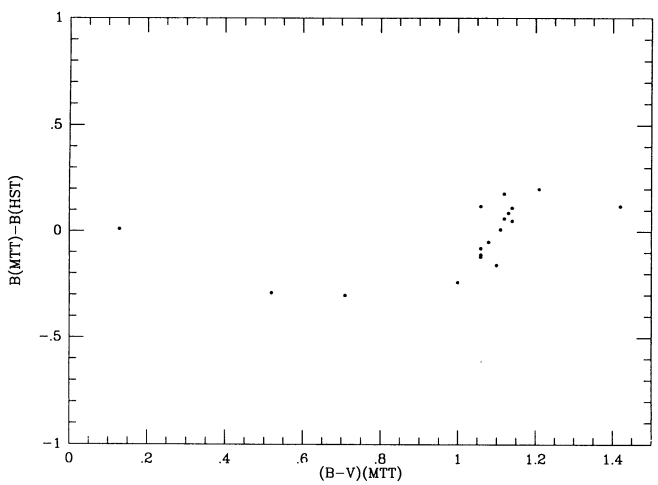

FIG. 4*a*

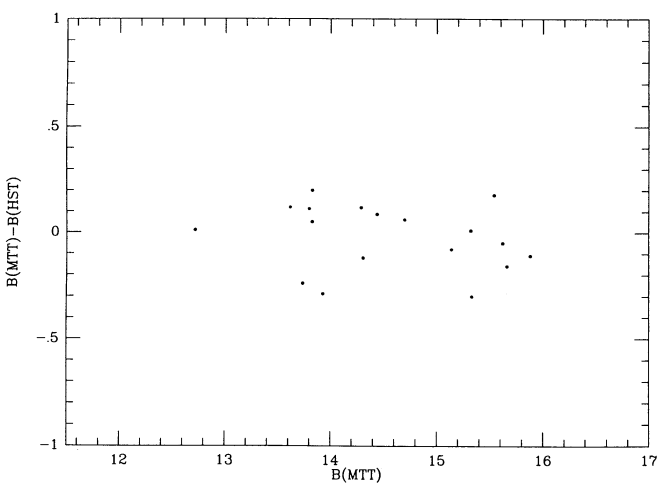

FIG. 4*b*

FIG. 4.—(*a*) Color equation plot for the *HST B* (F439W) image magnitudes compared to *B*-magnitudes for the stars in common from MTT (cf. Table 3. The mean difference is $\Delta B = -0.02$, with standard deviation $\sigma(\Delta B) = 0.16$ mag. (*b*) ΔB vs. B(MTT) for the same data.

TABLE 1

HST/PC CALIBRATED F439W *B*-PHOTOMETRY AND F469N He II PHOTOMETRY OF NGC 3603

HST Number	MTT/van den Bos	*X*	*Y*	*B*(*HST*)	*m*(469N)	HST Number	MTT/van den Bos	*X*	*Y*	*B*(*HST*)	*m*(469N)
1.....	12	764.0	37.0	13.69	13.69	40.....		700.0	523.7	14.28	14.20
2.....	18	929.2	93.7	14.43	14.27	41.....		690.7	532.8	14.94	14.98
3.....	32	621.0	131.5	15.31	15.37	42.....		698.5	535.0	13.89	13.82
4.....	41	756.3	169.5	15.82	15.96	43.....		602.6	535.0	14.96	14.84
5.....	13	327.2	197.9	13.50	13.55	44.....		733.5	536.1	16.01	16.15
6.....	29	1044.3	269.1	15.22	15.25	45.....		669.0	539.2	15.03	14.88
7.....	26	544.2	293.2	14.64	14.56	46.....		754.1	540.7	15.29	15.34
8, 9.....	21	832.2	299.0	15.64	15.57	48.....	14	1240.0	550.0	13.63	13.45
		803.2	315.3	14.79	14.86	49, 50.....	D[a]	680.9	550.2	13.73	13.71
10, 11.....	22	573.3	348.0	15.13	15.06			685.4	552.1	13.83	13.81
		596.0	359.8	15.59	15.50	51.....	23	872.9	558.2	14.35	14.34
12, 13.....	30	940.0	361.2	16.06	15.70	52, 53.....	D[a]	686.0	558.7	14.77	14.70
		964.8	363.7	16.09	16.33			689.4	559.0	15.38	15.18
14.....		678.3	386.0	14.97	15.00	54.....		705.7	560.0	15.68	15.82
15.....		662.4	389.0	16.28	16.43	55.....		669.5	581.4	15.98	16.14
16.....		735.9	407.2	14.62	14.61	56.....		657.0	582.0	15.69	15.63
17.....		679.8	418.1	15.13	15.08	57.....		664.2	594.0	15.07	14.95
18.....	C	719.0	442.9	12.66	12.32	58.....	15[b]	816.0	606.1	14.93	15.03
19.....	E	632.2	451.2	13.92	13.93	59.....		679.9	614.1	14.74	14.77
20.....		793.0	458.1	15.07	15.01	60.....		733.0	616.0	14.69	14.77
21.....		798.0	459.0	15.53	15.65	61.....	G,10	577.1	617.8	13.98	14.06
22.....	17	952.1	466.0	14.17	14.21	62.....	15[b]	784.9	630.0	14.36	14.37
23.....	B	715.0	475.1	12.12	11.45	63.....	40	1006.8	708.8	15.36	15.39
24.....	11	1339.0	476.9	13.78	13.75	64.....	16	50.8	1114.0	14.22	14.23
25.....		672.9	481.3	14.10	14.13	65.....	7	330.7	1205.4	12.71	12.92
26.....	A3	707.2	482.2	13.59	13.64	66.....		948.7	70.0	16.46	16.24
27.....		673.2	484.4	14.16	14.16	67.....	36	920.2	294.2	16.35	16.03
28.....		752.1	485.2	15.38	15.24	68, 69.....	44	808.2	396.1	16.41	16.13
29.....		677.0	487.0	14.77	14.90			828.0	400.3	16.83	16.80
30.....	A1	703.0	488.5	12.25	11.75	70.....		838.0	501.0	16.38	16.43
31.....	A2	710.0	492.2	13.10	13.11	71.....		899.6	522.0	16.47	16.62
33.....		729.0	495.3	14.17	14.08	72.....		917.0	561.0	16.94	16.86
34.....		536.0	501.7	15.42	15.25	73.....		687.4	330.0	17.05	16.55
35.....		576.0	504.5	15.83	15.68	74.....	45	363.3	415.1	15.99	15.77
36.....		666.0	511.0	15.48	15.29	75.....	35	137.1	532.9	15.63	15.31
37.....		657.7	520.5	14.98	14.85	76.....	39	366.8	923.3	15.67	15.72
38.....		633.5	522.0	14.12	14.08	77.....		728.0	533.0	15.91	15.68
39.....	F, 6	610.0	522.5	13.88	13.69						

NOTES.—HST numbers and *X*, *Y* coordinates (in *HST*/PC pixels: 1 pixel = 0".0439) refer to stars identified in Figs. 1 and 3, in order of increasing *Y* for HST 1–65. Letters are from van den Bos 1928 revised for star A by Hofmann & Weigelt 1986. F439W magnitudes for stars A1 and A2 (HST 30, 31) at the edge of a CCD frame are unreliable; we have obtained *B*(*HST*) from MTT-calibrated F555W *V*-photometry in the *HST* archives, after adding $(B-V) \simeq 1.09$, appropriate for cluster members in the core region (MTT). MTT 7, 16, 30, 35 = HST 65, 64, 12 or 13, 75 are nonmembers, according to MTT.

[a] Stars 49, 50, 52, and 53 together correspond to star "D."

[b] Stars 58 and 62 together correspond to star MTT 15.

b for R136, we find

$$\rho_a(R)/\rho_b(R) = 10^{c1a-c1b} f(c_{2b}-1)/f(c_{2a}-1) R^{c2a-c2b}$$

Substituting the above values for c_1, c_2 for each cluster, yields

$$\rho_a(R)/\rho_b(R) = 0.69 R^{-0.43} = 3.0^{+3.2}_{-2.2}$$

for the innermost bin centered on $R = 0.033$ pc. Thus, within the errors, both NGC 3603 and R136 have similar central *spatial* density.

We do not attempt to estimate the relaxation time of NGC 3603. It depends critically on the total number of stars, something about which we know very little, if anything, below 30 $M_\odot$ (see next section). In fact, the best way to probe the central mass distribution and hence also the effects of relaxation, is via velocity dispersion measurements of individual stars close to the center. We plan to attempt this with *HST* during cycle 4 for the core of NGC 3603, combined with ground-based CCD spectra, already obtained for a dozen stars outside the core.

3.3. *Initial Mass Function*

In order to derive the IMF, we must convert absolute magnitudes into mass. We do this following the recipe outlined by Drissen, Moffat, & Shara (1993), which makes use of the isochrones of Maeder & Meynet (1991) for solar metallicity (no *B*, *V* isochrones are available for $Z \approx Z_\odot/3$ as in 30 Dor, but the differences with $Z_\odot$ are small for massive blue stars) and an age of 3.2×10^6 yr, the youngest available, but also a reasonable compromise for the age of NGC 3603 (MTT). The results are shown in Figure 11, where a slope $d \log N(\log M)/d \log M = -1.4 \pm 0.6$, compared to a Salpeter value of -1.35 (albeit for 1–10 $M_\odot$ only). Thus, on the restricted observed interval 30–60 $M_\odot$, the IMF appears to be normal, within the rather poor limits of the errors. Note that comparable slopes emerge for 30 Dor in the LMC (-1.5 ± 0.2 for $M \geq 12 M_\odot$: Parker & Garmany 1993) and NGC 604 and 595 in M33 (-0.9 ± 0.2 for $M \approx 15$–$60 M_\odot$: Drissen et al. 1993).

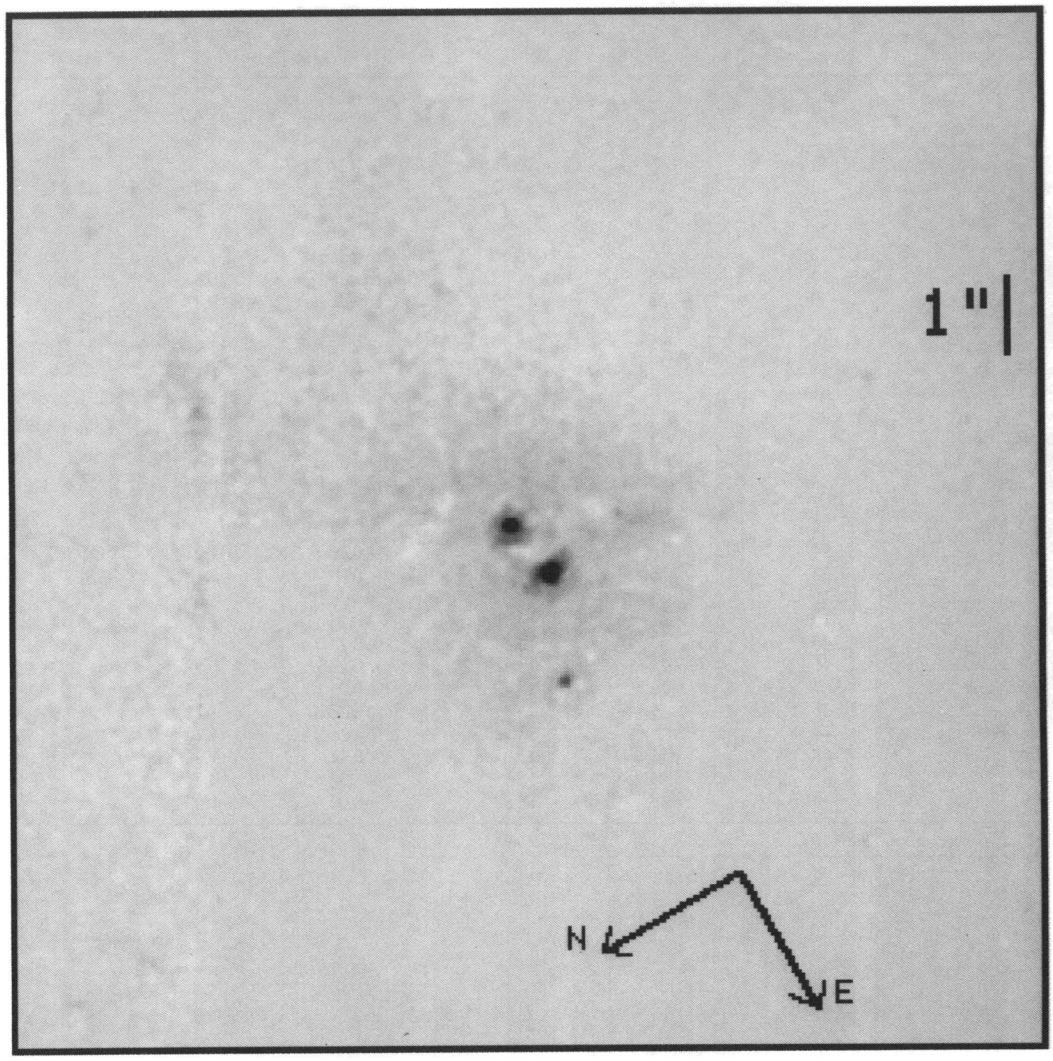

FIG. 5.—Net He II 4686 Å image (F469N − F439W × scaling factor), on same spatial scale as Fig. 2*a*

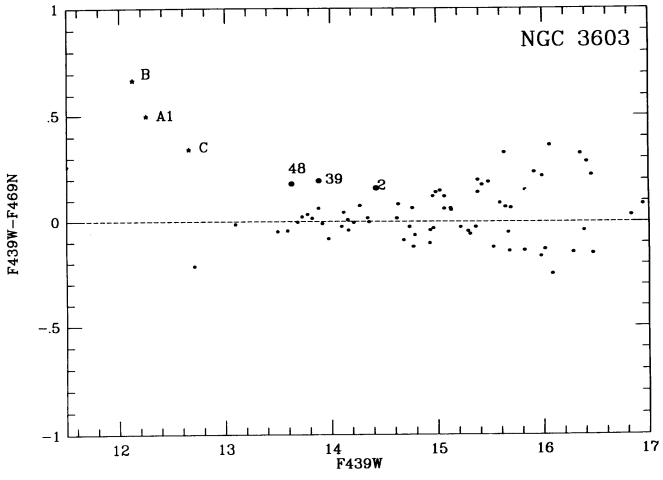

FIG. 6.—Normalized magnitude differences of narrow-band on-line (F469N) minus broadband *B* (F439W) magnitude vs. *B*(F439W) magnitude. Stars with strong He II 4686 emission will yield strong positive differences. The three WR stars (star symbols) and three strong-line Of or O(f) stars are indicated with *HST* numbers.

4. DISCUSSION

For stars of mass above 30 $M_\odot$, the core of NGC 3603 is marginally denser than the core of R136. This is significantly different from the factor 300 by which the core density of NGC 3603 was estimated to be greater than the core density of 30 Dor, deduced from ground-based data (MSS). Part of the reason for this difference is due to the fact that MSS based their estimate of the core density on the central *light* distribution. We now know that the core of NGC 3603 (unlike in R136) contains several exceptionally bright stars, which clearly biased the conversion of light into mass, using a normal IMF.

Beyond this relatively small difference in central density, NGC 3603 and R136 are quite similar both in stellar content and star density *profile* out to $r \sim 1$ pc, with no convincing indication of a flattened core down to the last bin centered at $r = 0.033$ pc. However, beyond $r \sim 1$ pc, NGC 3603 falls rapidly in density of massive stars, while R136 joins up with 30 Dor and continues with the same density profile out to over $r \sim 100$ pc. Thus, NGC 3603 can be considered to be essentially a clone of R136, without the presence of a massive, extended halo like the 30 Dor cluster around R136. At the

TABLE 2

HST STARS WITH GROUND-BASED PHOTOMETRY (MTT) OR SPECTRAL TYPES (MOFFAT 1983)

HST Number	MTT Number	van den Bos/Sher	B(MTT)	B(MTT) − B(*HST*)	$(B-V)$ (MTT)	Spectral Type (MOF)
1	12	23	13.80	+0.11	1.14	O9.5 Iab
2	18	22	14.31	−0.12	1.06	O5 V(f)
3	32	24	15.32	+0.01	1.11	...
4	41	49	15.66	−0.16	1.10	...
5	13	25	13.62	+0.12	1.42	B1.5 Iab
6	29	55	15.14	−0.08	1.06	...
7	26	64	14.70	+0.06	1.12	...
8, 9	21	60	14.66	(crowded)	1.33	...
10, 11	22	65	14.63	(crowded)	0.83	...
12, 13	30	58	15.29	(crowded)	0.47	...
19	...	E, 66?	...	...	...	O5 V
22	17	57	14.29	+0.12	1.06	O5 III(f)
24	11	47	13.83	+0.05	1.14	O4 V
23	...	B	...	...	...	WN6 + O5
26	...	A3	...	...	...	
30	...	A1	...	...	...	
31	...	A2	...	...	...	
39	6	F, 67?	12.85	(crowded)	0.99	O5.5 III(f)
49, 59 52, 53	...	D	...	...	...	O5 V
48	14	18	13.83	+0.20	1.21	O6 If
51	23	56	14.44	+0.09	1.13	O4 V(f)
58, 62	15	63	14.07	(crowded)	1.05	O5.5 V
61	10	G, 68	13.74	−0.24	1.00	O5 V
63	40	53	15.54	+0.18	1.12	...
64	16	28	13.93	−0.29	0.52	...
65	7	30	12.72	+0.01	0.13	...
67	36	59	15.51	(crowded)	1.11	...
68, 69	44	...	15.32	(crowded)	1.20	...
74	45	51	15.88	−0.11	1.06	...
75	35	26	15.33	−0.30	0.71	...
76	39	54	15.62	−0.05	1.08	...

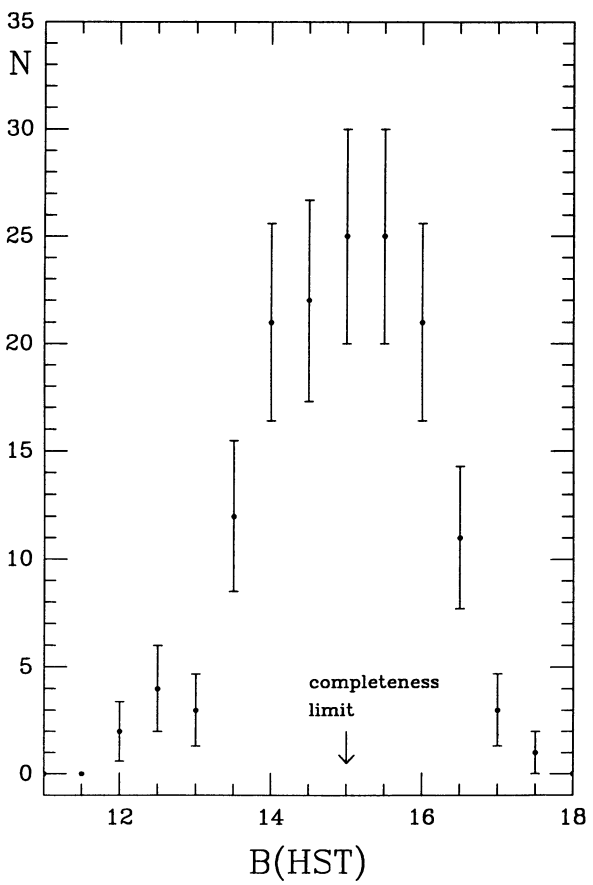

FIG. 7.—Number of stars vs. B-magnitude from Table 1. Bins are 1 mag wide. Errors are based on Poisson statistics.

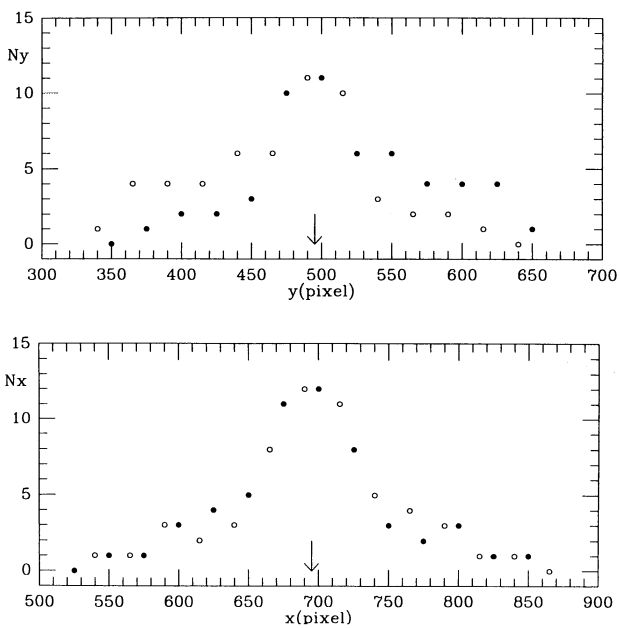

FIG. 8.—Strip counts in rectangles 240 pixels (perpendicular to the counting direction) by 50 pixels (in the counting direction), centered on initial approximate cluster center at $x = 700$, $y = 510$, for stars with $B \leq 15.0$ in Table 1. Filled circles refer to original points, open circles refer to reverse points after choosing a center of symmetry as indicated. Note the excess of stars near $y \sim 550$–600, caused by the clump of stars in and around component D.

TABLE 3

MEMBER STARS WITH $M_V \leq -5.0$ AND WITHIN 4 PARSECS OF THE CENTERS OF NGC 3603 AND R136

Star	r(pc)	B	M_V	Spectral Type
NGC 3603				
HST 30 = A1	0.015	12.25	−7.8	WR(+O?)
31 = A2	0.023	13.10	−6.9	...
26 = A3	0.026	13.59	−6.4	...
29	0.029	14.77	−5.2	...
27	0.037	14.16	−5.8	...
25	0.039	14.10	−5.9	...
23 = B	0.042	12.12	−7.9	WR(+O?)
40	0.044	14.28	−5.7	...
33	0.051	14.17	−5.8	...
41	0.057	14.94	−5.1	...
42	0.060	13.89	−6.1	...
37	0.067	14.98	−5.0	...
18 = C	0.085	12.66	−7.3	WR(+O?)
49	0.085	13.73	−6.3	
50 D	0.086	13.83	−6.2	O5 V
52	0.096	14.77	−5.2	
38	0.101	14.12	−5.9	...
19 = E	0.114	13.92	−6.1	O5 V
39 = F	0.133	13.88	−6.1	O5.5 III(f)
16	0.145	14.62	−5.4	...
43	0.149	14.96	−5.0	...
14	0.164	14.97	−5.0	...
59	0.179	14.74	−5.3	...
60	0.189	14.69	−5.3	...
62	0.242	14.36	−5.6	O5.5 V
58	0.245	14.93	−5.1	
61 = G	0.254	13.98	−6.0	O5 V
51	0.281	14.35	−5.6	O4 V(f)
9	0.313	14.79	−5.2	...
7	0.376	14.64	−5.4	...
22	0.385	14.17	−5.8	O5 III(f)
1	0.690	13.69	−6.3	O9.5 Iab
2	0.692	14.43	−5.6	O5 V(f)
5	0.705	13.50	−6.5	B1.5 Iab
48	0.816	13.63	−6.4	O6 If
24	0.960	13.78	−6.2	O4 V
MTT 25	1.15	14.63	−5.4	...
No more stars beyond this point				
R136				
pc6−9	0.006	12.85	−6.8	...
−1 = R136a-AS	0.015	12.78	−6.9	WR
−2 = R136a-AN	0.042	13.09	−6.6	WR
−5	0.079	13.73	−5.9	...
−8	0.080	14.28	−5.4	...
R136				
−4	0.089	13.56	−6.1	...
−7	0.089	13.78	−5.9	...
−10	0.102	14.51	−5.1	...
−3 = R136a-B	0.116	12.87	−6.8	WR
−13	0.142	13.92	−5.7	...
−20	0.160	14.58	−5.1	...
−11	0.169	13.58	−6.1	...
−6	0.176	14.06	−5.6	...
−32	0.197	14.30	−5.3	...
−23	0.203	14.15	−5.5	...
−38	0.287	14.52	−5.1	...
−36	0.315	14.47	−5.2	...
−29	0.389	14.21	−5.4	...
−41	0.408	14.59	−5.0	...
−27	0.413	13.83	−5.8	...
−34	0.437	14.32	−5.3	...
−30	0.438	14.26	−5.4	...
−40	0.442	14.54	−5.1	...
−31	0.443	14.28	−5.4	...
−43	0.464	14.61	−5.0	...
−33	0.477	14.31	−5.3	...
−26 = R136b	0.539	13.03	−6.6	Of?
−35	0.575	14.37	−5.3	...
−39	0.621	14.53	−5.1	...
−28	0.681	14.20	−5.4	...
−25 = R136c	0.858	12.86	−6.8	WR
−42	0.971	14.60	−5.0	...
−37	1.09	14.52	−5.1	...
−6015	1.27	14.21	−5.4	...
−6011	1.29	14.01	−5.6	...
−6012	1.96	14.08	−5.6	...
−6002 = Mk42	1.99	12.67	−7.0	O3 If/WN6 − A
−6017	2.28	14.40	−5.2	...
−6016	2.51	14.39	−5.2	...
−6004 = Mk34	2.66	12.95	−6.7	WN4.5
−6009	2.87	13.67	−6.0	...
−6001 = R134	2.90	12.57	−7.1	WN7
−6005 = Mk37W	2.91	13.30	−6.3	WN7 − A(Mk37)
−6013 = Mk33S	2.96	14.20	−5.4	WC5 + O4(Mk33)
−6018	2.99	14.47	−5.2	...
−6003 = Mk39	3.05	12.94	−6.7	O3 If/WN6 − A
−6007 = Mk37	3.07	13.46	−6.2	WN7 − A
−6006 = Mk35	3.12	13.36	−6.3	O3 If/WN6 − A
−6008	3.40	13.52	−6.1	...
−6014	3.43	14.21	−5.4	...
−6010	3.65	13.81	−5.8	...
−6019	4.19	14.57	−5.1	...

NOTES.—Data are sorted by increasing r. For NGC 3603: center at $(x_c, y_c) = (695, 495)$ pixels. With distance 7.0 kpc and 1 pixel = 0".0439 yields $r(\text{pc}) = [(x - x_c)^2 + (y - y_c)^2]^{1/2}$ (0.00149). With $B \leq 15.0$, $E_{B-V} = 1.44$, $V - M_V = 18.86$ and $M_B - M_V \approx -0.3$ for most of the (blue) member stars gives $M_V \leq -5.0$. For R136: center at $(x_c, y_c) = (346.26, 467.40)$ pixels (Campbell et al. 1992). With distance 52.5 kpc and 1 pixel = 0".0439 yields $r(\text{pc}) = [(x - x_c)^2 + (y - y_c)^2]^{1/2}$ (0.0112). With $V \leq 14.64$ and $V - M_V = 19.64$ gives $M_V \leq -5.0$, i.e., the same limit as for NGC 3603.

other extreme, one has the GHRs NGC 604 and 595 in M33, which lack a dominating nucleus.

While both NGC 3603 and R136 contain similar numbers of WR stars concentrated towards their dense centers, the WR stars in NGC 3603 are, on average, 1 mag brighter than those in R136. If this is not due to unresolved multiplicity, it might be a consequence of the slightly older age for NGC 3603 (earliest spectral type O4) compared to R136 (O3, if like the surrounding cluster). The most massive stars in very young clusters will not yet have had sufficient time to evolve away from and above the main sequence. On the other hand, there do exist brighter WR stars (e.g., R144) in 30 Dor *outside* R136 (Moffat 1989).

Why is a dense cluster like NGC 3603 so unique (hence rare) in the Galaxy, while R136/30 Dor is merely the youngest example of the LMC's numerous populous clusters? A clue to this difference might be the fact that the large-scale, disorganized motion of the ISM in the Galaxy (~ 10 km s^{-1}) is insufficient to form large stellar complexes via ram shock

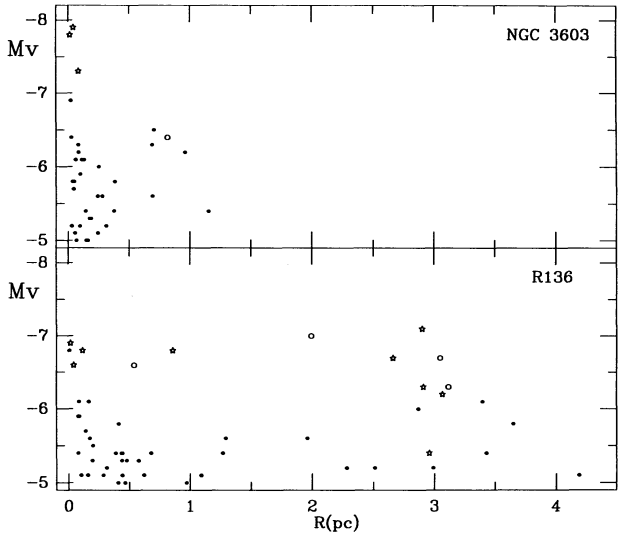

FIG. 9.—Magnitude vs. radius dependence out to $r \sim 4$ pc for $M_V \leq -5.0$ of stars in NGC 3603, compared to R136. Data are from Table 3 (taken from Tables 2 and 4 of Campbell et al. 1992 for R136). WR stars are indicated by star symbols, Of/WR and Of stars by open circles.

TABLE 4

RADIAL PROJECTED STAR COUNTS OUT TO $R = 4$ pc IN NGC 3603 (MEMBERS ONLY) AND R136/30 DOR FOR $M_V \leq -5.0$

			log σ	
r_i (pc)	r_o (pc)	log $\bar{r}$ (pc)	NGC 3603	R136
0	0.050	−1.48	$3.01^{+0.13}_{-0.20}$	$2.58^{+0.19}_{-0.36}$
0.025	0.075	−1.27	$2.80^{+0.12}_{-0.17}$	$1.80^{+0.31}_{-\infty}$
0.050	0.100	−1.11	$2.53^{+0.13}_{-0.20}$	$2.23^{+0.18}_{-0.30}$
0.075	0.150	−0.93	$2.23^{+0.12}_{-0.18}$	$2.12^{+0.14}_{-0.20}$
0.10	0.20	−0.81	$1.93^{+0.13}_{-0.19}$	$1.87^{+0.14}_{-0.20}$
0.15	0.30	−0.63	$1.52^{+0.14}_{-0.21}$	$1.45^{+0.16}_{-0.22}$
0.20	0.40	−0.51	$1.27^{+0.14}_{-0.21}$	$1.03^{+0.17}_{-0.31}$
0.30	0.60	−0.33	$0.55^{+0.20}_{-0.37}$	$1.15^{+0.11}_{-0.15}$
0.40	0.80	−0.21	$0.30^{+0.20}_{-0.37}$	$0.90^{+0.11}_{-0.15}$
0.60	1.20	−0.03	$0.25^{+0.15}_{-0.22}$	$0.17^{+0.16}_{-0.25}$
0.90	1.70	+0.13	$-0.51^{+0.23}_{-0.52}$	$-0.21^{+0.18}_{-0.30}$
1.30	2.30	0.27	$-\infty$	$-0.58^{+0.19}_{-0.36}$
1.80	3.00	0.39	$-\infty$	$-0.26^{+0.12}_{-0.17}$
2.40	4.00	0.51	$-\infty$	$-0.39^{+0.11}_{-0.14}$

NOTE.—Projected density $\sigma = N/A$, where $N \pm (N)^{1/2}$ is the number of stars in a bin $r_i < r \leq r_o$ of mean radius

$$\bar{r} = \int_{r_i}^{r_o} r^2\, dr \Big/ \int_{r_i}^{r_o} r\, dr\,. \quad A = \pi(r_o^2 - r_i^2)$$

compression, compared to the larger dispersion in the LMC (50–100 km s^{-1}) (Kumai, Basu, & Fujimoto 1993a; Kumai, Hashi, & Fujimoto 1993b).

If objects like NGC 3603 are common in other galaxies, their detection will be very difficult because of their extremely compact nature, causing potential confusion with single bright stars. Thus, its proximity in the Galaxy, even compared to R136 in the LMC, makes NGC 3603 a very useful target for the study of young stellar clusters of ultra-high density. Clearly, we require even higher spatial resolution than we have demonstrated here to verify whether the bright central stars of NGC 3603 are in fact multiple objects, leading to yet a higher star density.

This work was supported in part by grants from NSERC (Canada) and FCAR (Quebec) to A. F. J. M. L. D. is grateful to NSERC (Canada) for a postdoctoral fellowship, and expresses his appreciation for a STScI postdoctoral fellowship provided by the STScI Director's Discretionary Research Fund.

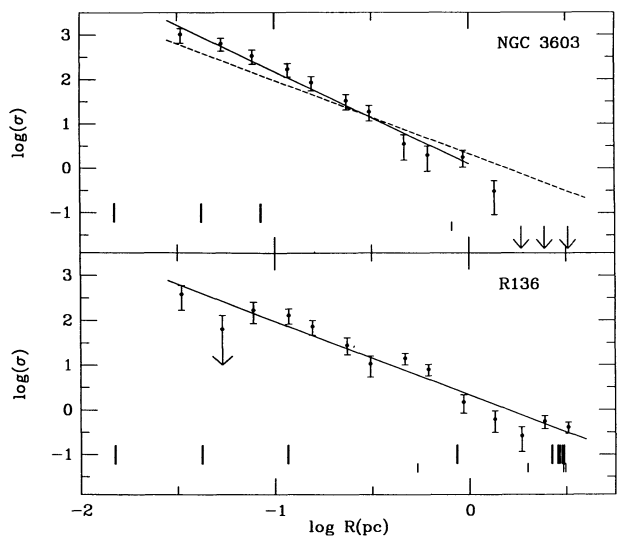

FIG. 10.—Radial dependence of star number surface density in NGC 3603 and R136 for stars of $M_V \leq -5.0$, in both cases. Data are taken from Table 3. Straight lines are weighted fits (out to $\log r = -0.03$ only for NGC 3603, after which the counts plummit). Positions of known WR stars are shown by long thick vertical bars, strong-line Of-stars by short thin vertical bars for each cluster. Note that the inner three bars refer to WR stars in both cases.

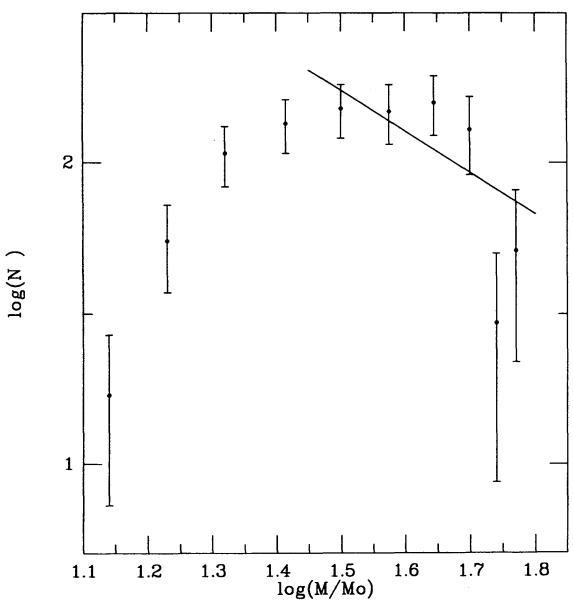

FIG. 11.—Initial mass function $N(\log M)$ vs. $\log M$ for members of NGC 3603. The straight line is a weighted fit for $M \approx 30$–$60\ M_\odot$, with slope -1.4 ± 0.6.

REFERENCES

Baier, G., Eckert, J., Hofmann, K.-H., Mauder, W., Schertl, D., Weghorn, H., & Weigelt, G. 1988, Messenger, 52, 11
Baier, G., Ladebeck, R., & Weigelt, G. 1985, A&A, 151, 61
Campbell, B., et al. 1992, AJ, 104, 1721
Drissen, L., Moffat, A. F. J., & Shara, M. M. 1993, AJ, 105, 1400
Eckart, A., Genzel, R., Hofmann, R., Sams, B. J., & Tacconi-Garman, L. E. 1993, ApJ, 407, L77
Elson, R. A. W., Freeman, K. C., & Lauer, T. R. 1989, ApJ, 347, L69
Harris, H. C., Baum, W. A., Hunter, D. A., & Kreidl, T. J. 1991, AJ, 101, 677
Hofmann, K.-H., & Weigelt, G. 1986, A&A, 167, L15
Krabbe, A., Genzel, R., Drapatz, S., & Rotaciuc, V. 1991, ApJ, 382, L19
Kumai, Y., Basu, B., & Fujimoto, M. 1993a, ApJ, 404, 144
Kumai, Y., Hashi, Y., & Fujimoto, M. 1993b, ApJ, 416, 576
Maeder, A., & Meynet, G. 1991, AAS, 89, 451
Melnick, J., Tapia, M., & Terlevich, R. 1989, A&A, 213, 89 (MTT)
Moffat, A. F. J. 1983, A&A, 124, 273
———. 1989, ApJ, 347, 373
Moffat, A. F. J., & Niemela, V. S. 1984, ApJ, 284, 631
Moffat, A. F. J., Niemela, V. S., Phillips, M. M., Chu, Y.-H., & Seggewiss, W. 1987, ApJ, 312, 612
Moffat, A. F. J., Seggewiss, W., & Shara, M. M. 1985, ApJ, 295, 109 (MSS)
Parker, J. W., & Garmany, C. D. 1993, AJ, 106, 1471
Rieke, G. H., & Rieke, M. J. 1988, ApJ, 330, L33
Vacca, W. 1990, Ph.D. thesis, Univ. Colorado
van den Bos, W. H. 1928, Bull. Astron. Inst. Netherlands, 4, 261
Walborn, N. 1973, ApJ, 182, L21
Welch, W. J., et al. 1987, Science, 238, 1550